High power mm-wave loss measurements of ITER ex-vessel waveguide components at the FALCON test facility at the Swiss Plasma Center

Timothy P. Goodman[1,*], *Humberto* Torreblanca[1], *Cinta* Marraco Borderas[1], *René* Chavan[1], *Avelino* Mas Sanchez[1], *Anastasia* Xydou[1], *Mario* Cavinato[2], and *Katarina* Cindric[2]

[1]Ecole Polytechnique Fédérale de Lausanne (EPFL), Swiss Plasma Center (SPC), CH-1015 Lausanne, Switzerland
[2]Fusion for Energy, Josep Pla 2, Torres Diagonal Litoral B3, E-08019 Barcelona, Spain

Abstract. Many future fusion devices will rely heavily, if not solely, on electron cyclotron (EC) heating subsystems to provide bulk heating, instability control (neoclassical tearing mode (NTM) stabilization), and thermal instability control. Efficient use of the installed heating power (gyrotrons) requires low-loss transmission of the power over 100s of meters since the mm-wave sources need to be installed where the stray magnetic field has a small amplitude. Transmission lines are used to propagate the mm-wave power over this long distance. Quasi-optical techniques (mirrors) are used at W7X and are planned for DTT, for example. Guided components are installed at DIII-D, TCV and elsewhere and are planned at JT60SA and ITER. High power test facilities exist to evaluate the power transmission of assemblies of guided components (transmission lines). The European test facility FALCON was setup by Switzerland and Fusion for Energy (F4E) in Lausanne Switzerland at the Swiss Plasma Center (SPC) in the Ecole Polytechnique Fédérale de Lausanne (EPFL). Operations are funded through a framework contract with F4E. SPC operates the facility. Two ITER-class 170GHz gyrotrons are housed within the facility and used to evaluate the thermal behaviour of components provided by various ITER partners. Loss measurements are presented for miter bends and waveguides of several materials at two different diameters. The results are used to model the expected losses in the ITER ex-vessel waveguides (EW) of all five EC launchers.

1 Introduction

The use of electron cyclotron (EC) heating at the fundamental through 3rd harmonic resonance in fusion experiments [1–6] and future devices [7–9] is well established and is expected to expand significantly to also include electron Bernstein wave heating [10]. EC power is transmitted over 10s or 100s of meters from the gyrotron sources to the launching antennas via quasi-optical mirrors or evacuated over-moded corrugated transmission lines (TLs). In the latter, at high power, power losses are measured to exceed the theoretical losses associated with the lowest loss LP_{01} mode. While the fractional losses are still low, the designs of cooling systems for multimegawatt plant systems depend on the expected losses. Experimental confirmation of the heat transfer coefficients (HTC) between cooling structures and the objects that are being cooled is commonly required. In the same way, confirmation of the power losses within the objects is needed.

Loss measurements in high-power, long-pulse experiments have been reported in, for example, [11–13]. Infrared temperature measurements are made of relatively long TLs. Uncooled waveguides (WGs) store the heat during the pulse, dependent on the thermal mass of the components. Calorimetry is based on the total change in temperature of the components from the start to the end of the mm-wave pulse (when linear) and/or the integral of the flow and water temperature difference when cooled. The latter is used for the mitre bend (MB) mirrors.

Experiments, at QST (formerly JAEA) in Japan, using General Atomics, 63.5mm inner-diameter, corrugated aluminum alloy 6061-T6 WG and MBs, found an exponential decay of the temperature away from the MBs and enhanced losses far from the MBs, even when considering the higher losses resulting from some LP_{11} mode content in the transmitted beam [14–16]. The importance of reflections from the high-power mm-wave calorimetric loads used during transmission measurements has been cited in previous tests [11] and demonstrated recently [13]. Reflections lead to higher heating of the TLs over long distances, but the reflected power level is difficult to quantify. Simulations of the Ohmic attenuation losses from the EC beam including the expected mode content of the ITER TL between the gyrotron MOU and the diamond window of the EW are consistent with the ITER transmission requirements [17]. The ITER loss specification for the TL is 0.05%/m and reported values have ranged from 0.012%/m to 0.028%/m at in inner diameter $\varnothing$=63.5mm (the Ohmic losses scale as $\varnothing^{-3}$ [18], so they are expected to be 2 × larger in the $\varnothing$=50mm waveguide used in the ITER TL).

In this paper we discuss loss measurements of new waveguide manufactured by a European consortium under contract with Fusion For Energy. They were de-

signed according to the ITER specifications for the ex-vessel waveguides (EW) of the ITER launchers (4 upper launchers (UL) - mostly dedicated to neoclassical tearing mode (NTM) stabilization and other current profiling techniques - and one equatorial launcher (EL) for central heating and current drive). The waveguides are uncooled and are made of aluminium alloy 6061-T6 (Al), stainless steel 316L (SS) and CuCr1Zr copper alloy. They have 50mm inner-diameter, are corrugated and evacuated, and incorporate integrated couplings that house double spring-energized all-metal seals to meet the stringent ITER vacuum requirement. For the experiments reported here, only the inner seal is used. (The outer seal creates a service-vacuum space that allows automated vacuum leak testing, at ITER.) In addition to the straight waveguide sections, tests of CuCr1Zr mitre bends are presented.

The ITER EC section has allocated certain levels of loss (specified as transmission efficiencies or transmitted power minimums) to various portions of the EC plant to meet the overall efficiency required by the ITER project. The EW subsystem must have 98% transmission efficiency. The power losses presented here are consistent with this requirement when used to calculate the estimated losses of the EW. Additionally, the data is used to design the EW cooling system to ensure stable, reliable, operation even when fully powered. The theoretical loss rate for the Al waveguides is 0.0048%/m; but, as in previous experiments [11, 16], the measured loss is nearly an order of magnitude higher.

2 Measurement layout

The FALCON experimental zone is housed in one hall of the Swiss Plasma Center. The zone is delimited by a protective wall preventing human access during operation of the gyrotron, transmission line and dummy loads. The available space for testing equipment is (width x length x height) 10m x 12m x 6m.

Each of the two gyrotron towers houses a 1MW-class ITER-like gyrotron operating at 170GHz. An evacuated, 8.534m-long, 63.5mm-inner-diameter, Al TL with 2 MBs, manufactured by General Atomics (GA), connects the MOU of a Thales Electron Devices (TED) gyrotron [19, 20] to a spherical load developed by IFP-CNR [21] to allow long-pulse (1000s), high-power testing (950kW demonstrated) . This is the so-called EU TL; it is 1.9m off of the false floor of the testing area.

A GYCOM gyrotron occupies the second tower and its MOU is connected to a similar TL that starts at a similar height as the EU TL, then zig-zags down to 0.81m off of the false floor via 3 MBs to bypass the support tower of the TED gyrotron, and after ≈2.2m bifurcates in an RF switch (180°, or 90° bend) graciously provided by GA. The 90° branch of the switch has been used to test a GA RF load [22]. The through branch (180°) connects to a downta-per from 63.5mm to 50mm inner diameter. This is used for ITER UL component testing and is the so-called ITER TL. Figure 1 shows a panaramic view of the TLs. Only the TED gyrotron and its MOU are seen at the left; the GYCOM gyrotron and MOU are hidden from view. The devices under test (DUTs) start with an MB manufactured by SPC [23] on the lower TL in Fig. 1. Further information about the facility is found in [12].

From the input of this MB, eighteen different combinations of components have been installed over the past 3 years, allowing comparisons of the behaviour of components to each other. The longest series of components in the ITER TL is 9.584m and is terminated by a GYCOM RF load. Shorter combinations were terminated by a second spherical dummy load (20 cooling channels per hemisphere as opposed to 16-channels for the IFP-CNR load, so-called RFL.20 and RFL.16, respectively). All loads measure the same RF power for the same gyrotron operational parameters within the error bars of the measurements: approximately ±3%.

The rest of this paper is divided into sections addressing different types of power losses in a typical transmission line system. Section 3 discusses the mitre bend, in which the beam is reflected from a mirror to affect a change in direction. Mitre bends at FALCON incorporate thermocouples in the mirrors to diagnose losses and beam alignment (see [23]). Section 4 details experiments made using stainless steel waveguides. These are particularly lossy and have low thermal diffusivity, allowing visualization of the underlying heat flux in a way not possible with typical waveguide materials. Losses in waveguide far from miter bends, which act as a source of higher order modes near cut-off (here refered to as very high order modes VHOMs), yield a measure of the nearly constant baseline heat flux; these are discussed in Section 5. Load reflections are also discussed in Section 5 before conclusions drawn from this work are summarized in Section 6.

3 Mitre Bends

Two mitre bends have been manufactured by SPC. Both MB mirrors are equipped with a pair of thermocouples (TCs) that are 1mm below the reflecting surface and are 4mm on either side of the mirror center. Four additional TCs are embedded in the MB body. In addition, calorimetry is made separately on the mirror and body water cooling circuits. Measurements of the losses in both the mirror and body of the MB confirm that the two MBs are identical within experimental accuracy when installed at the same location in the ITER TL (i.e. as the first MB). This allows them to be used as measurement devices when placed at different locations in the TL: Any differences in losses are due to the TL configuration and not the component itself.

The GYCOM load must be oriented vertically. The load and its required preload are, together, 2.5m tall; therefore, a second miter bend is positioned below the load (see Fig. 2). In this TL, the first MB reflects in the E-plane and the second, under the load, in the H-plane. According to theory, mirror losses are half as large in the H-plane for these 90° MBs [24]. As described in [23], the RF beam (and therefore the heat flux) is not centered on the first MB, so there is a significant temperature difference at the two TC locations (≈50±6°C); however, at the location of the second MB the temperature difference is reduced (≈25°C
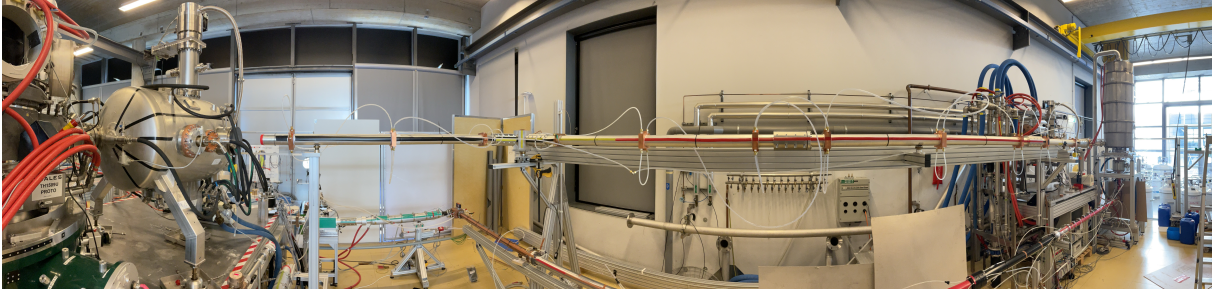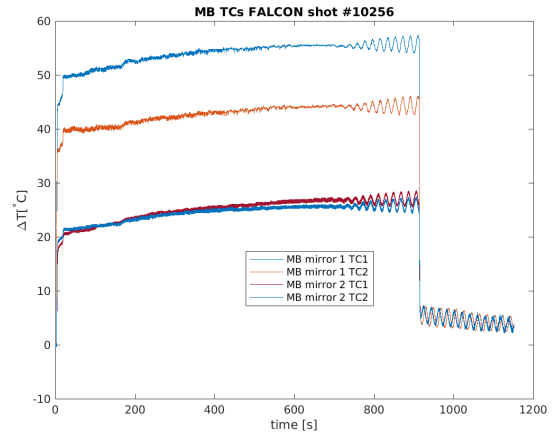
Figure 1. The FALCON test facilities 2 TLs: EU TL (upper in 63.5mm inner diameter Al) and ITER TL (lower with switch and downtaper - covered in green tape - to 50mm inner diameter multi-material).
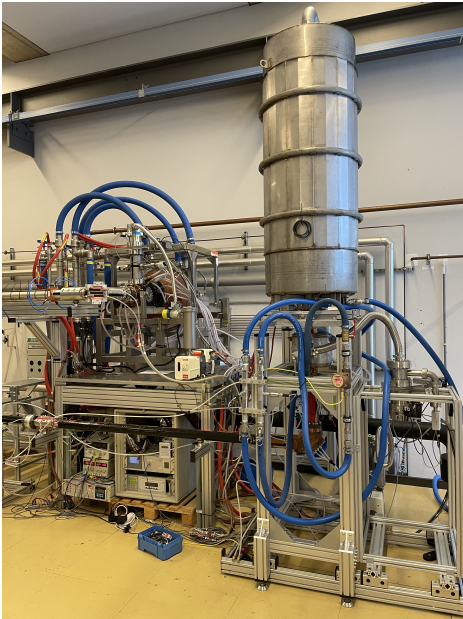
Figure 2. The GYCOM preload and load (stainless steel) positioned above an SPC MB (CuCr1Zr) connected by a 0.34m-long CuCr1Zr waveguide covered in red electrical tape and preceded by a 2m-long stainless-steel waveguide convered in black electrical tape.

Figure 3. The temperature difference traces of the thermocouples from two mitre bends, one in E-plane (higher temperatures) and one in H-plane (lower temperatures). The beam is off-center on mirror 1 and more centered on mirror 2. The average temperature of mirror 1 is approximately twice that of mirror 2, as expected.

average, see Fig. 3) and we conclude that the beam is more centered.

As described above, it has been verified that these TCs and their acquisition chain have an identical response to the same input RF beam [23]. Figure 3 shows the difference in temperature (relative to the start of the pulse) of each thermocouple in the MB mirrors for a 15-minute-long, 0.51MW RF pulse. A fast step in acceleration voltage in the gyrotron causes a step in RF power at $\approx$10s and the fast response is seen on the TCs ($1/e$ response time $\approx$0.5s [23]). The slow rise over time, starting before $\approx$200s, is due to re-circulation of warm cooling water and the oscillations at the end of the pulse are due to the feedback control of the heat exchangers in the closed loop cooling system. From independent water temperature measurements of the MB mirror and body, in which the time-changing input water temperature is subtracted, calorimetry shows that the total power loss in the MB as-

sembly is 0.35% of the transmitted power; with 22% of that power lost in the MB body.

4 Stainless Steel WGs

Two stainless steel (SS) WGs are available to compare to WGs made of other materials. They both show significant and identical axial variations in temperature on a spacial scale less than their 1.2m length when positioned at the same location in the TL. This was an unexpected result since neither the Al nor the CuCr1Zr WG showed such variations when positioned at the same location in the TL. Because of the very low heat diffusivity in SS, the WGs can be used as a diagnostic. Despite the relatively short TL, these WGs permit measurements "far" from a MB as described below.

It is known that the beam in the TL is not a pure LP_{01}, but is a mix of several low order LP_{mn} modes as shown in Fig. 5 of Ref. [23] and indicated by the off-set of the beam on the MB. Having noticed that the distance between the temperature peaks in the spacial pattern corresponds to several of the half-beat-wavelengths of the measured

modes in the TL, experiments were carried out to change the mode mixture and measure potential changes in the temperature pattern in the SS WGs. To this end, the mirror alignment in the MOU was changed in several steps, while under vacuum. By measuring the power losses in the MOU and the temperature difference between TCs in the MB, it was verified that the original alignment could be recovered after the experiment.

Figure 4 shows measurements of the temperature rise in the MOU cooling water for 3 shots; for the original mirror alignment, a misaligned mirror and the recovered mirror alignment. Power losses are listed in the legend. The mirror was misaligned in steps to lower the difference between the mirror TCs temperature. Falcon shot 8935 has a more-central beam alignment on the MB mirror; the temperature difference between the TCs was lowered from ±13% to ±4.4%. However, the MOU losses increased concomitantly.
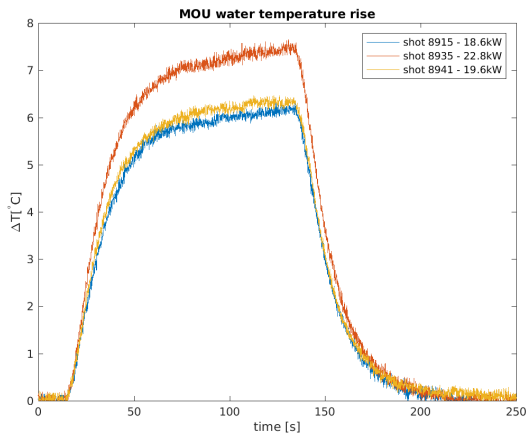
Figure 4. Temperature increase in the MOU cooling water for the original mirror alignment (#8915), misaligned mirror (#8935) and recovered position (#8941). The associated power losses are given in the legend.

The axial temperature profiles of the two SS WGs positioned imediately after the first MB are shown in Fig. 5. The relatively massive coupling between the two WGs is seen as a deep notch in the temperature curves. The data is taken from an Infra-red camera viewing both the front side and back side (using a large reflector plate). Several TCs are placed along the WGs to cross-calibrate the IR images. The temperature is higher in the misaligned case and the shape of the profile is different. The next highest order mode (LP_{11}) is excited by angles in the input beam coupled from the MOU. It has a beat wavelength with the LP_{01} mode of 3.14m. Significant changes in the RF heating pattern can be expected at 1/4 of this length (0.79m).

The short-scale-length temperature variations are superimposed on a curve that decreases monotonically away from the MB (at z=0 in Fig. 5). Previous investigators have modeled this as an exponential decay in the heating due to modes near cut-off that are generated in the MB. We refer to these as very high order modes (VHOMs). Here
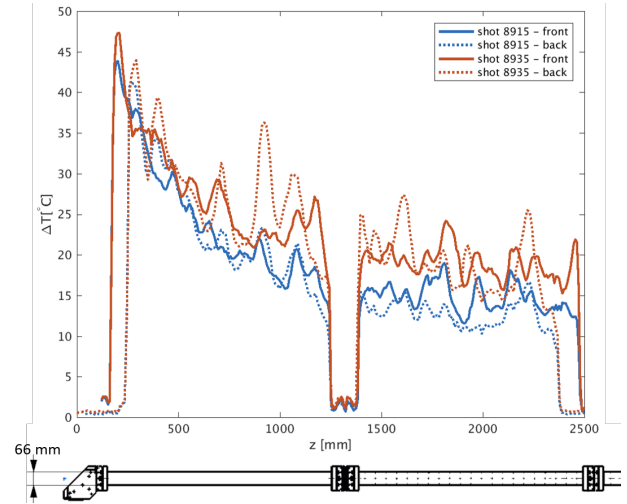
Figure 5. The change in the axial temperature profiles for the original (8915) and misaligned shots (8935) shown in Fig. 4 for both the front (solid) and back (dashed) side. SS WGs show the change in the TL heating pattern when the MOU mirror is misaligned. The relatively high thermal mass coupling between the waveguides appears as a notch centered at ≈1300mm, and at each end. (N.B. The drop in ΔT at each end of the "back" side, shifted with respect to the front side, is due to the size of the reflector - the back is not longer visible to the camera at the extremes.) A sketch of the miter bend and stainless steel waveguides with couplings is shown below the graph.

we model the WG heating with a constant baseline heating plus heat flux decaying exponentially with z. The model parameters are the result of fitting the data from several shots. Figure 6 compares the measured and modelled temperature profile for the longer FALCON shot 8942 (pulse lengths are typically limited by the maximum allowed WG temperature - set here to 80°C to protect the aluminum-sheathed, spring-loaded, metallic vacuum seals).
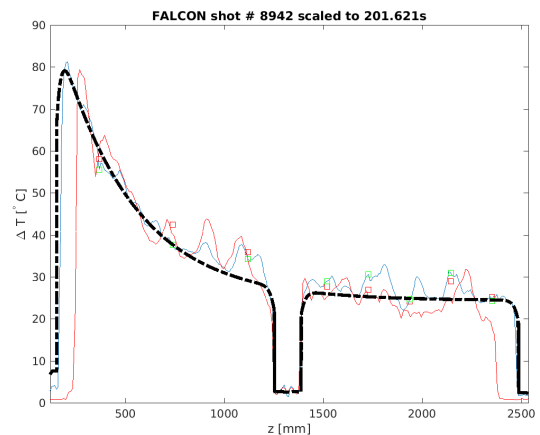
Figure 6. The simulated temperature difference resulting from a simple off-set exponential heat flux model (dashed line), compared to the measured axial temperature (blue-front, red-back, red squares - TCs) for a longer pulse in which the MOU mirror was slightly readjusted to better match the original alignment.)

The decay length in the model is found to be 0.37m, whereas the combined length of the two SS WGs is 2.5m; thus, all of the power associated with the VHOMs is absorbed in these two WGs. This forward propagating VHOM power constitutes 1/4 of the total mode conversion loss in a WG [25] and can be determined by integrating the exponential, knowing the fit parameters. Similarly, at the output of the 2nd WG the temperature rise is due solely to the baseline heat flux in the WG. From the fit parameters, we find the baseline WG absorption rate is a factor of 7.3 to 8.1 times theory, and the VHOM generation is between 1.2 and 2.3 times the theoretical predictions. The relatively large range in the values is a result of the different MOU alignments.

Determination of the decay length was not possible using the CuCr1Zr or Al WGs, for example, as it becomes of the same order as the length of the WG components (scaling inversely with the surface resistivity i.e. $\sqrt{\sigma_{CuCr1Zr}/\sigma_{SS}}$, where σ is the electrical conductivity). Similarly, the presence of HOMs is not evident in the WGs with high heat diffusivity; no significant azimuthal temperature variation was measured as these WGs cannot sustain the high temperature gradients seen in Fig. 5 (e.g front to back as well as axially).

Determination of the decay length (and baseline losses) in materials other than SS depends on scalings based on the relative conductivity (1/resistivity) of the material.

On the other hand because the VHOMs are eliminated by the SS WGs, it may be possible to directly measure the baseline heating in other WG materials placed downstream from the SS WGs, effectively "far" from the MB (source of VHOMs).

5 WGs far from MBs

COMSOL™ [26] thermal simulations were carried out for three WGs placed after the SS WGs, where the internal heat flux is due solely to the enhanced baseline heating. The room temperature of 20°C has been subtracted from the simulation temperature presented in Fig. 7. They are compared to measured temperature-difference profiles for 3 shots at different powers. A constant heat flux (along the axis) is applied in each simulation to match the measurements of the first WG (in CuCr1Zr, given in the figure legend as hfluxCCZ). The simulated loss rate is equivalent to 0.052%/m for each shot. The second WG is in Al and the third in (thinner-walled) CuCr1Zr, followed by a short, thick walled CuCr1Zr waveguide and the RFL.20. (The hfluxCCZ is scaled to simulate higher losses in Al, as described below.)

The heating appears to be significantly over-estimated in the simulation for the Al WG (centered at 6m in Fig. 7). We note that by chance the simulated temperature (dark blue line) for the first shot matches the measured temperature (magenta line) for the second shot. This indicates that the simulation overestimates the temperature in Al by a factor $\frac{302kW}{211kW} = 1.43$ relative to measurements.

The theoretical ratio of losses ($\sqrt{\sigma_{CuCr1Zr}/\sigma_{Al}} = 1.30$) and the inverse ratio of the thermal masses

$((mc_p)_{CuCr1Zr}/(mc_p)_{Al} = 1.43)$, where m is the mass and c_p the heat capacity, have already been taken into account in the simulations (i.e. $\Delta T_{Al} \approx 1.86\Delta T_{CuCr1Zr}$, as seen in Fig. 7). So, it appears that surface resistances of the two materials are nearly the same (i.e. the factor 1.3 is not required for the simulation to match the measured Al temperature). Alternately, the losses in the CuCr1Zr WG could be underestimated.

Subsequent conductivity measurements in the 80-100GHz frequency range in a Fabry-Perot resonance cavity configuration using samples of the 3 WG materials, as well as a reference oxygen-free high-conductivity Cu sample, confirm the higher than expected surface resistance (aternatively, lower than expected conductivity) of the CuCr1Zr.

Using the measured conductivity, the expected LP_{01} loss rate in the corrugated CuCr1Zr WG is 0.0046%/m; so, the simulations indicate a baseline heating enhancement of 11, perhaps even higher nearer the load. This exceeds the enhancement factor of 7.7 in SS WG and suggests an additional $\approx 47\%$ contribution from reflected power from the load even at a distance of ≈ 4.5m.

Without a knowledge of the absorption rate of the reflected power in the WG, it is difficult to integrate the total reflected power and thereby quantify the load reflection coefficient ($P_{reflected}/P_{incident}$). Low power load reflection measurements, using vector network analyser with extension heads for 170GHz operation attached to a Gaussian Optics Lens Antenna (GOLA) to couple to ⌀=50mm WG at the input of the load, appropriately time-gated to remove the effects of the GOLA and associated WG, gave 0.010% at 170GHz and 0.1% at 169.68GHz (covering the gyrotron frequency-drift range during pulses of up to 1MW). However, this measurement methodology may not capture well all the HOMs generated by the RFL.20; therefore, these constitute a lower bound for the reflections.

Previous modeling [12] postulated 0.7% reflection. And measurements in a test setup for JT60SA [13] indicate that the influence of an additional preload extends ≈17m from the preload location back towards the gyrotron in ⌀60.3mm Al 6061-T6 waveguide. Our CuCr1Zr waveguide has similar losses to this material. From this, if we postulate a decay length of ≈ 4m for load reflections, we cannot resolve the difference in the enhancement factors between the stainless steel and the other waveguides; a much shorter decay of 1.4m is required. In that case, we derive the pair (load reflection, baseline loss enhancement): ≈ (0.52%, 6.8×) i.e. a load reflectivity of ≈ -23dB. However, if this pair of parameters is used in the COMSOL™ model, does it match the measured temperatures along all of the waveguides?

Using this pair of parameters for the load reflection and baseline loss enhancement, COMSOL™ modeling shows a reasonably good fit to the measured temperatures only at the same waveguides used to determine the enhancement (i.e. the SS WGs and the CuCr1Zr waveguide at the left in Fig. 7). The simulated waveguide temperatures nearer the load (at the right in Fig. 7) strongly exceed the measured temperatures making this an unreliable measurement of the load reflection.
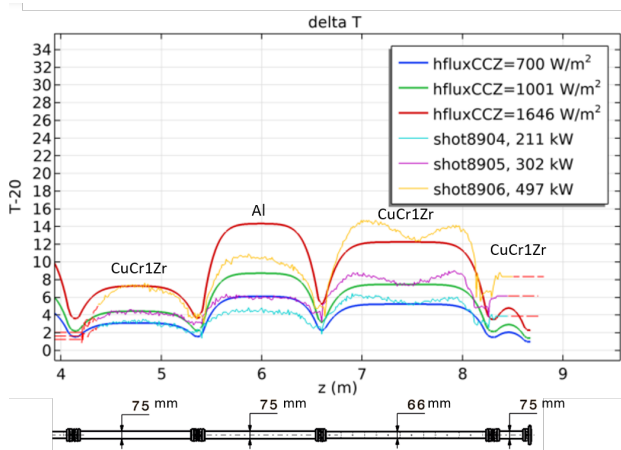
Figure 7. COMSOL™ simulated temperature (thick lines) and measured temperature (thin lines) for three different transmitted powers (see legend). Three WGs are simulated at their axial locations (z) relative to the MB: left - CuCr1Zr (outer diameter = 75mm), middle - Al (o.d. = 75mm), right - CuCr1Zr (o.d. = 66mm). The couplings are seen as notches (not as steep as with SS WGs - see Fig. 6). The heat flux in CuCr1Zr is 520W/MW/m. The heat flux in Al is scaled with conductivity as described in the text. A sketch of the waveguides with couplings is shown below the graph.

6 Conclusions

We have shown that MB manufacturing is very reproducible allowing MBs to be used as diagnostics when equipped with TCs in the mirror and body.

Stainless steel waveguides are also useful as diagnostics, showing localised heating due to mode beating that is masked in high-conductivity components. The thus-determined mode structure can be modified by altering the beam alignment at the TL input.

Because of its relatively high resistivity, decay lengths of MB-generated VHOMs are measurable in relatively short SS components. Scaling the measured decay length to CuCr1Zr WGs yields 1.7m - longer than most of the available components. It was not possible to measure the decay length in these components reliably.

Two SS WGs together dampen all VHOMs from the MB allowing a good determination of the baseline heating "far" from a MB - both in the SS and, with a different measurement setup, in CuCr1Zr. Similarly the total forward traveling VHOM power from the MB was determined by integration of the best-fit simplified model curves. An enhancement of between 1.3 and 2.3 is found above theoretical expectations (depending on the beam alignment).

Comparison of the measurements from different materials has proved useful. First, a high-frequency measurement of the CuCr1Zr surface resistance, or conductivity, helped explain the lack of significant difference between Al and CuCr1Zr component heating. Second, resolving the difference in baseline enhancement leads to an estimate of the reflected power from the RFL.20 of ≈ -23dB; albeit raising a different discrepancy in the measurements (over-estimate of WG temperatures near the RFL.20). De-

spite the latter, it is clear that even small power reflections can dominate power loss measurements in the short transmission line tested at FALCON, as evoked in experiments elsewhere (e.g. [11] and references therein). Estimates of the reflection coefficient of the ITER Upper Launcher [27] are similar to those discussed here for the load.

These enhancement results were used to calculate the expected losses in the EW of all five EC launchers for ITER, showing that the present design meets the ITER allocation of losses.

References

[1] S. Alberti, K.A. Avramidis, W. Bin, A. Bertinetti, J. Dubray, D. Fasel, S. Garavaglia, J. Genoud, T. Goodman, J.P. Hogge et al., *High-efficiency, long-pulse operation of MW-level dual-frequency gyrotron, 84/126GHz, for the TCV Tokamak*, in *2019 44th International Conference on Infrared, Millimeter, and Terahertz Waves (IRMMW-THz)* (2019), pp. 1–2

[2] S. Moriyama, T. Kobayashi, A. Isayama, M. Terakado, M. Sawahata, S. Suzuki, K. Yokokura, M. Shimono, K. Hasegawa, S. Hiranai et al., Nuclear Fusion **49**, 085001 (2009)

[3] M. Cengher, J. Lohr, P. Simmerling, Y. Gorelov, A. Torrezan, D. Ponce, J. Doane, D. Su, X. Chen, IEEE Transactions on Plasma Science **48**, 1698 (2020)

[4] D. Wagner, J. Stober, M. Kircher, F. Leuterer, F. Monaco, M. Münich, M. Schubert, H. Zohm, G. Gantenbein, J. Jelonnek et al., *Commissioning of the extended multi-frequency ECRH system at AS-DEX upgrade*, in *2017 42nd International Conference on Infrared, Millimeter, and Terahertz Waves (IRMMW-THz)* (2017), pp. 1–2

[5] H. Laqua, A. Leggieri, C. Lechte, D. Moseev, F. Legrand, G. Gantenbein, H. Oosterbeek, H. Braune, I. Chelis, J. Jin et al., *The ECRH-Power Upgrade at the Wendelstein 7-X Stellarator*, in *21st joint workshop on electron cyclotron emission (ECE) and electron cyclotron resonance heating (ECRH)* (2022)

[6] L. Delpech, *A new 3MW ECRH system at 105 GHz for WEST*, in *21st joint workshop on electron cyclotron emission (ECE) and electron cyclotron resonance heating (ECRH)* (2022)

[7] B. Bigot, Nuclear Fusion **62**, 042001 (2022)

[8] M. Tran, P. Agostinetti, G. Aiello, K. Avramidis, B. Baiocchi, M. Barbisan, V. Bobkov, S. Briefi, A. Bruschi, R. Chavan et al., Fusion Engineering and Design **180**, 113159 (2022)

[9] A. Romano, B. Baiocchi, L. Balbinot, W. Bin, A. Bruschi, D. Busi, A. Bussolan, M. De Nardi, F. Fanale, P. Fanelli et al., *The design of the ECRH system of DTT*, in *21st joint workshop on electron cyclotron emission (ECE) and electron cyclotron resonance heating (ECRH)* (2022)

[10] S.J. Freethy, L. Figini, M. Henderson, H. El-Haroun, S. Gibson, K.K. Kirov, A. Köhn-Seeman, I. Konoplev, S. Saarelma, R. Sharma et al., EPJ Web Conf. (2022)

[11] J. Anderson, J. Doane, H. Grunloh, R. O'Neill, R. Ikeda, Y. Oda, K. Takahashi, K. Sakamoto, Nuclear Fusion **57**, 056030 (2017)

[12] T.P. Goodman, M. Cavinato, R. Chavan, A. Más-Sanchez, P.S. Silva, M. Vagnoni, T. Tersztyanszky, S. Carre, IEEE Transactions on Plasma Science **48**, 1537 (2020)

[13] T. Kobayashi, H. Yamazaki, S. Hiranai, M. Sawahata, M. Terakado, K. Ishita, J. Hinata, F. Sato, K. Wada, R. Ikeda et al., Fusion Engineering and Design **175**, 113009 (2022)

[14] R. Callis, J. Doane, H. Grunloh, K. Kajiwara, A. Kasugai, C. Moeller, Y. Oda, R. Olstad, K. Sakamoto, K. Takahashi, *Testing of ITER-class ECH transmission line components at the JAEA radio-frequency test stand*, in *Proc. 23rd IAEA Fusion Energy Conf., Republic of Korea* (2010)

[15] K. Takahashi, K. Kajiwara, Y. Oda, A. Kasugai, N. Kobayashi, K. Sakamoto, J. Doane, R. Olstad, M. Henderson, Review of Scientific Instruments **82**, 063506 (2011)

[16] J.P. Anderson, J.L. Doane, H.L. Grunloh, R.W. Callis, R. Ikeda, Y. Oda, K. Takahashi, K. Sakamoto, Journal of Infrared, Millimeter, and Terahertz Waves **37**, 55 (2016)

[17] M.C. Kaufman, C. Lau, G.R. Hanson, Journal of Infrared, Millimeter, and Terahertz Waves **39**, 456 (2018)

[18] E.A. Nanni, S.K. Jawla, M.A. Shapiro, P.P. Woskov, R.J. Temkin, Journal of Infrared, Millimeter, and Terahertz Waves **33**, 695 (2012)

[19] A. Leggieri, D. Bariou, V. Hermann, F. Legrand, G. Lietaer, C. Lievin, R. Marchesin, P. Thouvenin, F. Albajar, F. Sanchez et al., *Th1509U European 170 Ghz 1 Mw Cw Industrial Gyrotron Upgrade* (IEEE, New York, 2021), IEEE International Vacuum Electronics Conference IVEC

[20] T.P. Goodman, S. Alberti, J. Genoud, H. Torreblanca, F. Albajar, F. Sanchez, A. Leggieri, F. Legrand, C. Liévin, Z. Ioannidis et al., 47th International Conference on Infrared, Millimeter and Terahertz Waves (IRMMW-THz) **Delft, The Netherlands** (2022, 28 August – 2 September)

[21] W. Bin, A. Bruschi, F. Fanale, M. Francesca, F. Lucca, F. Albajar, S. Alberti, G. Carannante, M. Cavinato, I. Chelis et al., Fusion Engineering and Design **146**, 36 (2019)

[22] Anderson, James, Doane, John, Moeller, Charles, Grunloh, Howard, O´Neill, Raymond, Brookman, Michael, Smiley, Matthew, Su, David, EPJ Web Conf. **203**, 04001 (2019)

[23] A. Xydou, T.P. Goodman, R. Chavan, M. Vagnoni, H. Torreblanca, M. Cavinato, Fusion Engineering and Design **170**, 112457 (2021)

[24] M.K. Thumm, W. Kasparek, IEEE Transactions on plasma science **30**, 755 (2002)

[25] J. Doane, J. Anderson, H. Grunloh, W. Wu, Fusion Engineering and Design **93**, 1 (2015)

[26] *Comsol multiphysics® v. 6.0, comsol ab, stockholm, sweden*, www.comsol.com.

[27] T.P. Goodman, *Rf stray radiation estimation in upper launcher (yc4ntv v1.0)*, https://user.iter.org/default.aspx?uid=YC4NTV